NREL
NATIONAL RENEWABLE ENERGY LABORATORY

Development and Commissioning of a Small/Mid-Size Wind Turbine Test Facility

Preprint

D. Valyou, T. Arsenault, K. Janoyan, and P. Marzocca
Clarkson University

N. Post
National Renewable Energy Laboratory

C. Grappasonni, M. Arras, and G. Coppotelli
University of Rome Sapienza

D. Cárdenas and H. Elizalde
Tecnológico de Monterrey Campus Ciudad de Méx

O. Probst
Tecnológico de Monterrey

To be presented at AIAA SciTech 2015
Kissimmee, Florida
January 5–9, 2014

Conference Paper
NREL/CP-5000-63051
January 2015

Contract No. DE-AC36-08GO28308

NOTICE

This report is available at no cost from the National Renewable Energy Laboratory (NREL) at www.nrel.gov/publications.

Available electronically at http://www.osti.gov/scitech

Available for a processing fee to U.S. Department of Energy and its contractors, in paper, from:

U.S. Department of Energy
Office of Scientific and Technical Information
P.O. Box 62
Oak Ridge, TN 37831-0062
phone: 865.576.8401
fax: 865.576.5728
email: mailto:reports@adonis.osti.gov

Available for sale to the public, in paper, from:

U.S. Department of Commerce
National Technical Information Service
5285 Port Royal Road
Springfield, VA 22161
phone: 800.553.6847
fax: 703.605.6900
email: orders@ntis.fedworld.gov
online ordering: http://www.ntis.gov/help/ordermethods.aspx

Cover Photos: (left to right) photo by Pat Corkery, NREL 16416, photo from SunEdison, NREL 17423, photo by Pat Corkery, NREL 16560, photo by Dennis Schroeder, NREL 17613, photo by Dean Armstrong, NREL 17436, photo by Pat Corkery, NREL 17721.

Development and Commissioning of a Small/Mid-Size Wind Turbine Test Facility

Daniel Valyou[1], Tyler Arsenault[2], Kerop Janoyan[3], and Pier Marzocca[4,5]
[1,2,3,4] *Clarkson University, Potsdam, NY, 13699, USA*
[5] *Royal Melbourne Institute of Technology University, Bundoora VIC 3083 Australia.*

Nathan Post[6]
National Renewable Energy Laboratory, Golden, CO, 80401, USA

Chiara Grappasonni[7], Melissa Arras[8], and Giuliano Coppotelli[9]
University of Rome Sapienza, 00184 Rome, Italy

Diego Cárdenas[10] and Hugo Elizalde[11]
Tecnológico de Monterrey Campus Ciudad de México, D.F. CP14380, México

and

Oliver Probst[12]
Tecnológico de Monterrey, Campus Monterrey, CP64849, México

This paper describes the development and commissioning tests of the new Clarkson University/Center for Evaluation of Clean Energy Technology Blade Test Facility. The facility is a result of the collaboration between the New York State Energy Research and Development Authority and Intertek, and is supported by national and international partners. This paper discusses important aspects associated with blade testing and includes results associated with modal, static, and fatigue testing performed on the Sandia National Laboratories' Blade Systems Design Studies blade. An overview of the test capabilities of the Blade Test Facility are also provided.

I. Introduction

Wind turbine blades are designed to capture wind effectively to deliver maximum energy production; however, manufacturing and logistic constraints require wind turbine blades to be made as light and affordably as possible. As a result, these highly stressed structures are subjected to variable and stochastic dynamic environmental loads during their operational life, which can lead to catastrophic failure. For example, rotor blades comprise roughly 7% of total wind turbine components failures[1], as shown in Figure 1. During operation, large and frequent fluctuations in wind intensity and direction can cause severe strain on wind turbine blades. Wind turbine blade failures impact safety, cause turbine downtime, and can pose a risk to individuals located within the vicinity of wind turbines. Safety is of particular concern when considering small and mid-size wind turbines, as they are often located in residential, commercial, and community areas in close proximity to the public. Current standards (Table 1) do not require extensive physical testing of small wind turbine blades; however, static and fatigue structural testing is required for

---

1 Blade Facility Manager, MAE Dept., 8 Clarkson Ave, Potsdam, NY, 13699-5725, AIAA Member.
2 PhD Student, 8 Clarkson Ave, Potsdam, NY, 13699, AIAA Member.
3 Associate Professor, CEE Dept., 8 Clarkson Ave, Potsdam, NY, 13699, AIAA Senior Member.
4 Professor, MAE Dept., 8 Clarkson Ave, Potsdam, NY, 13699-5725, AIAA Associate Fellow.
5 Professor and Deputy Head of School (Aerospace and Aviation), PO Box 71 Bundoora VIC 30833 Australia, AIAA Associate Fellow.
6 Engineer (Blade Testing), National Wind Technology Center, 15013 Denver West Parkway, Golden, CO, 80401.
7 Post-Doc Associate, AIAA Member.
8 PhD Candidate, Dipartimento di Ingegneria Meccanica e Aerospaziale, Via Eudossiana, 18, AIAA Student Member.
9 Assistant Professor, Dipartimento di Ingegneria Meccanica e Aerospaziale, Via Eudossiana, 18, AIAA Associate Fellow.
10 Assistant Professor, Mechatronics Engineering Department, Calle del Puente 222 Col. Ejidos de Huipulco Tlalpan.
11 Professor, Mechatronics Engineering Department, Calle del Puente 222 Col. Ejidos de Huipulco Tlalpan.
12 Professor, Physics Department, Av. Eugenio Garza Sada 2015 Sur, Col. Tecnológico.

the blades of wind turbines with more than a 200-m^2 swept area, which is typically a blade length of >8 meter (m) for horizontal-axis wind turbines. As deployment of small and community wind turbines expands, it is important to ensure that testing methods and facilities are available to evaluate blade designs for performance, reliability, and safety.

Wind manufacturers, operators, investors, insurance companies, and wind farm developers will benefit from third-party testing, inspection, and evaluation of small and mid-size wind turbine blades. Third party review of design, manufacturing and testing serve to extend the life cycle of wind turbine blades and minimize the risks from design flaws and manufacturing defects; however, there are few blade test facilities worldwide and their capabilities for testing wind turbine blades focus on current standards and primarily serve the market for large wind turbines. As a result, this scarcity makes it difficult and costly for small and mid-size blade manufacturers to test their products.

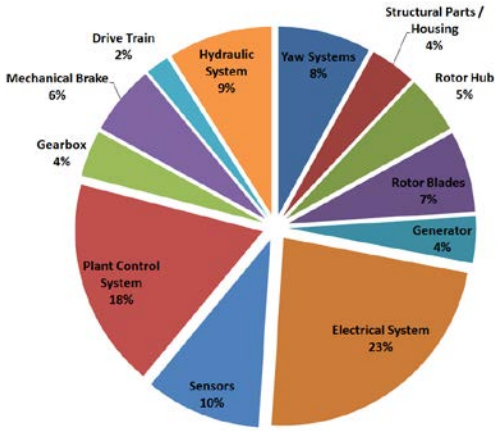

Figure 1. Share of major wind turbine component failures.[1]

With this current reality in mind, and with the goal of extending the life cycle of small wind turbines and minimizing the potential for failures, a grant from the New York State Energy Research and Development Authority (NYSERDA) established the Center for Evaluation of Clean Energy Technology (CECET) and created the opportunity to develop the small-to-mid-size wind turbine Blade Test Facility (BTF), installed and operated by Clarkson University. The facility will help manufacturers test their blades to American Wind Energy Association (AWEA) and international design standards, in particular to the International Electrotechnical Commission (IEC) 61400–2, Wind turbines – Part 2: Design requirements for small wind turbines, and IEC 61400-23 "Wind turbines - Part 23: Full-scale structural testing of rotor blades," among others (Table 1).

Table 1. Partial list of small wind turbine testing standards

North America:	
Standard	**Title**
AWEA 9.1	Small Wind Turbine Safety and Performance
CAN/CSA C61400-2	Wind Turbines - Part 2: Design Requirements for Small Wind Turbines
International:	
Standard	**Title**
EN/IEC 61400-2	Wind Turbines - Part 2: Design Requirements for Small Wind Turbines
MCS 006	Product Certification Scheme Requirements: Micro and Small Wind Turbines
RUK 2014 (formerly British Wind Energy Association 2008)	RenewableUK Small Wind Turbine Standard

The BTF leverages ongoing collaborative efforts with national laboratories such as the U.S. Department of Energy's (DOE) National Renewable Energy Laboratory (NREL), the Massachusetts Clean Energy Center's Wind Technology Testing Center, international partners such as the University of Rome Sapienza, the Instituto Tecnológico y de Estudios Superiores de Monterrey, and private industry partners. The BTF performs full-scale structural testing of wind turbine blades up to 15 m in length, such as static and dynamic load testing, blade experimental structural analysis including mass, stiffness, and modal testing, structural materials characterization, and structural design and analysis support. The BTF also supports industry participation and continuing education through distance learning and workforce development programs.

II. BTF Description

The BTF test cell consists of an 8-m x 14-m strong floor with two 6-m-wide x 5-m-high reaction walls. The reaction walls are designed to sustain a moment of 1.02 Mega-Newton meters (MN-m), and the floor can sustain 445 kilonewtons (kN) of tensile load. Both the strong floor and reaction walls are equipped with anchorages or tie-downs positioned 1.2 m apart in a uniform grid. The reaction walls' support has two test stands (to run simultaneous static and fatigue tests) to perform testing of full-scale wind turbine blades up to 15 m, scaled turbines blades above 15 m, and sub-scale blade components up to 15 m in length. Blade tests are performed with purpose-built structural test and data acquisition equipment, sourced from MTS Systems Corporation, and modal test equipment from LMS Testing Solutions and PCB Piezotronics, global leaders in mechanical testing and measurement equipment. Additional test equipment for the test cell includes a range of hydraulic actuators, hydraulic power supply, servo controllers, two 250-kip (1.1 MN) modular test frames, a 220-kip (979 kN) Instron testing frame, and a 110-kip (489 kN) MTS test frame. For certification, blade testing is performed in accordance with IEC standards, and certification services are provided by Intertek.

The facility performs structural testing of turbine blades and substructures, including static, forced displacement and resonant fatigue, bi-axial fatigue, and static and fatigue torsion testing. It is modular in design and incorporates a range of servo-hydraulic actuators and test fixtures, load cells, and a variety of high-resolution data acquisition systems. Multiple actuators can be deployed to approximate a distributed load to test articles. In addition, the BTF control system incorporates a number of safety features, including load, displacement, error, and data acquisition limits in software, as well as mechanical load abort and load-limiting systems. The control system also incorporates facility power-quality monitoring and UPS protection, which safely parks the test article in the event of a power quality event. These safety features protect test articles from excessive loads, displacements, and issues with grid power quality. A dedicated MTS data acquisition system allows for simultaneous recording of all measurement channels such as strains, loads, and deflections during the test. Furthermore, the BTF utilizes instruments required for precision measurement and nondestructive testing along with visual inspections to monitor the condition of the wind turbine blades. Figure 2 shows the facility's layout.

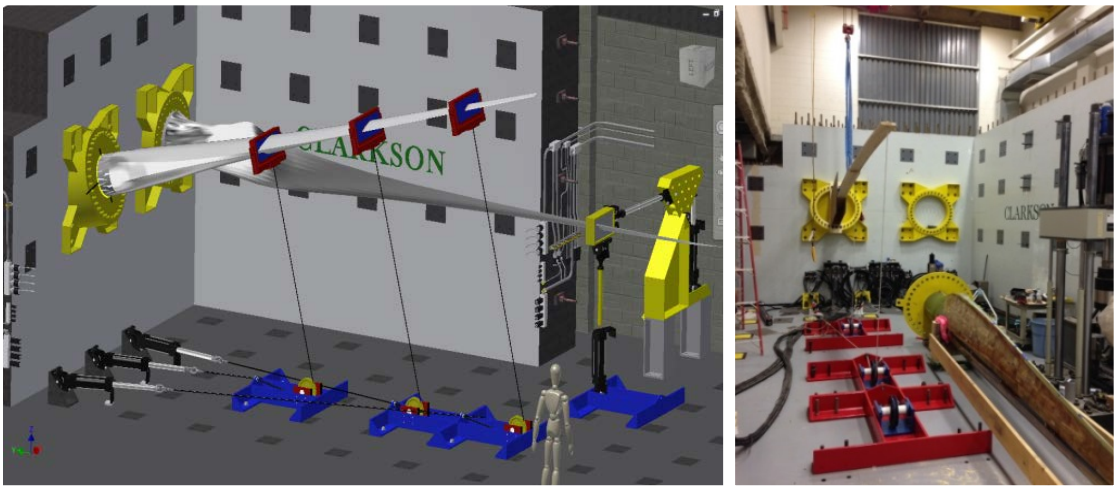

Figure 2. Layout of the Clarkson/CECET Blade Test Facility. Side view (left) and end view (right) showing the commission blade on the floor and a wood beam used to verify control of the hydraulics mounted on one test stand.

A. Test Control

The MTS FlexTest 60 controller is an eight-channel, two-station real-time controller with eight valve drivers, eight universal signal conditioners, eight channels of A/D input, eight channels of D/A output, a dual-serial interface, a 16-channel digital input/output, two hydraulic service manifold controllers, and a hydraulic power unit control. Test control is accomplished with AeroPro test control software, which allows for closed-loop independent control of each actuator, including running multiple simultaneous tests. The system is capable of supporting a wide variety of hydraulic actuators, both dynamic and quasi-static. In addition, the facility currently incorporates six static actuators ranging in stroke length from 0.8 m to 1.6 m and capable of loads up to 67 kN, and two dynamic actuators with a full-range stroke of 0.6 m and a load capacity of 25 kN.

B. Data Acquisition System

The BTF data acquisition hardware consists of the MTS FlexTest 60 controller, the MTS FlexDac data acquisition (DAQ) system, and the LMS SCADAS DAQ. The FlexTest controller captures the load, actuator displacement, and draw wire displacement transducers through eight 494.26 digital universal conditioners. These conditioners have 19-bit A/D, full-range signal conditioners, a 122.88-kilohertz (kHz) sample rate, and digital filtering with computer-controlled range, zero, excitation, filtering, and shunt calibration. The FlexDac data acquisition collects the strain data for the blade and consists of 128 channels of 24-bit simultaneous data acquisition, with a synchronization timer input between the FlexDac and the controller, with each input capable of quarter, half, full bridge, analog voltage, and Transducer Electronic Data Sheet (TEDS) input with bridge completion, software selectable hardware filtering, signal conditioning, and an external shunt resistor. The FlexDac data acquisition and FlexTest data acquisition are synchronized for a unified time signature. The LMS SCADAS system measures and analyzes the accelerometer data for modal analysis and is a 48-channel, 24-bit, simultaneous data acquisition system that accepts voltage, ICP, AC/DC bridge, and active sensors with a frequency range and filtering optimized for vibration measurement. Each system is connected to its own independent UPS to ensure clean and constant power delivery. A summary of the BTF instrumentation is provided in Table 2.

Table 2. BTF Instrumentation

• 16 Channel FlexTest Controller	• 48 Channels Accel or Bridge DAQ
• 8 Valve Drivers	○ 24 Bit Resolution
• 8 Digital Universal Conditioners	○ 512 KHz Sample Rate
• 16 Channels A/D	○ Voltage or ICP input
• 8 Hydraulic Actuators w/ Load Cell	• Ethernet Interface
• 3 Dynamic Actuators	• Test Lab Advanced Software
• 5 Static Actuators	○ Impact Testing
• 3 Service manifolds	○ MIMO FRF Testing
• 128 Channel FlexDAC System	
• AeroPro DAQ software	
○ 24 Bit Resolution	
○ 6 KHz Sample Rate	

The system sensors include a range of load cells for the hydraulic actuators, draw wire extensometers up to 5 m in length for quasi-static displacement measurements, resistive and piezoelectric strain gauges, accelerometers, inclinometers, linear variable differential transformers and temposonic displacement transducers to accommodate a wide array of test setups. The test control and instrumentation block diagram is shown in Figure 3.

1. Strain Gauge Instrumentation

The strain gauge type typically used by the CECET BTF is the uni-axial gauge Vishay L2A-06-125LT-350 and 90° rosettes Vishay L2A-06-250LW-350. These gauges were selected to have a 350-Ohm gauge resistance, allowing for higher excitation voltage, and a self-temperature-compensation appropriate for composite materials. Each channel is wired to the DAQ in a three-wire quarter bridge configuration to compensate for wire length resistance. Half or full bridge gauge configurations are also accommodated by the DAQ system, but increase the cost of the gauges.

BTF strain gauge channel names are in the form:

GXX-YYYYY-AA-ZZZ

where XX is the gauge number, YYYYY is the span location of the gauge in mm, and AA is a letter code indicating location as follows:

HP –High-pressure spar cap of the blade
LP – Low-pressure spar cap of the blade
LE – Leading edge (nose) of the blade
TE – Trailing edge of the blade
ZZZ is the angle of the gauge relative to the span axis of the blade in degrees (typically 000, 045, 090, or 135).

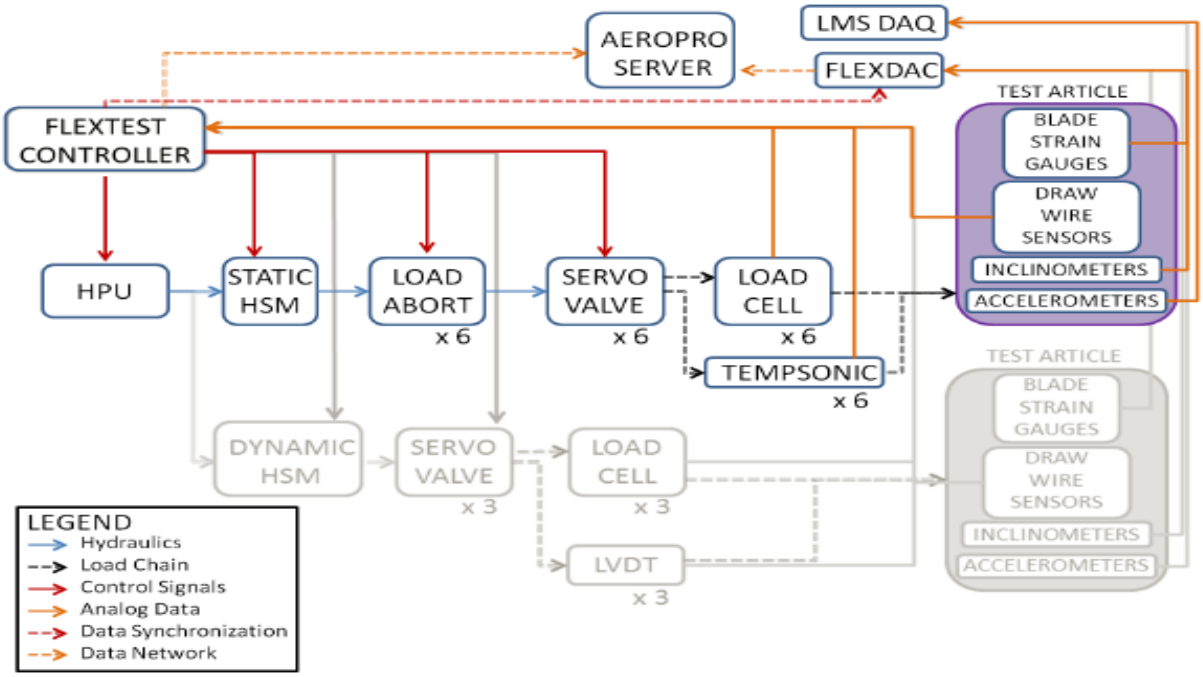

Figure 3. Instrumentation and control block diagram (static test highlighted).

The instrumentation plan for Sandia National Laboratories' Blade Systems Design Studies (BSDS) blade used in commissioning the BTF is shown in Figure 4.

2. Other Test Instrumentation

When testing a blade at the BTF, displacement is measured using Micro Epsilon analog draw wire displacement transducers with analog voltage output. The calibration scale factor is verified for each transducer against an externally calibrated steel rule prior to running a test. For the BSDS blade, each draw wire displacement transducer was located so the draw wire runs parallel to the loading cable. Actuator displacements are measured with tempsonic (static test) or Linear Variable Differential Transformer (LVDT) transducers. Actuator displacement is used as the primary displacement limit measurement. Applied force(s) are measured using load cells, which also provide control feedback. A shunt calibration check and verification with a calibrated load is performed prior to introducing the load cell into the load chain. Ambient temperature and humidity is measured in the laboratory at the test stand using a relative humidity/temperature transmitter. This device is calibrated by an external lab on an annual basis and is connected to an analog input of the FlexDac.

C. Test Hardware

1. Wall Mount and Adapter Plate

The adapter plate is a two-piece modular design consisting of the wall mount and blade adapter. The wall mount is a high-strength structural steel fixture that is capable of supporting any typical blade up to 15 m in length (shown in Figure 6). It is designed to support a bending moment of 2 MN-m. The blade adapter is specific to each test article, with the wall mount's 1.219-m bolt circle of 36 1.25-inch-12 threaded studs for its outer ring and a bolt circle compatible with the test article for the inner ring, shown in Figure 5. Hardware components are designed to sustain the ultimate failure load for a given test with a minimum safety factor of 2.5, as analyzed using a finite-element analysis.

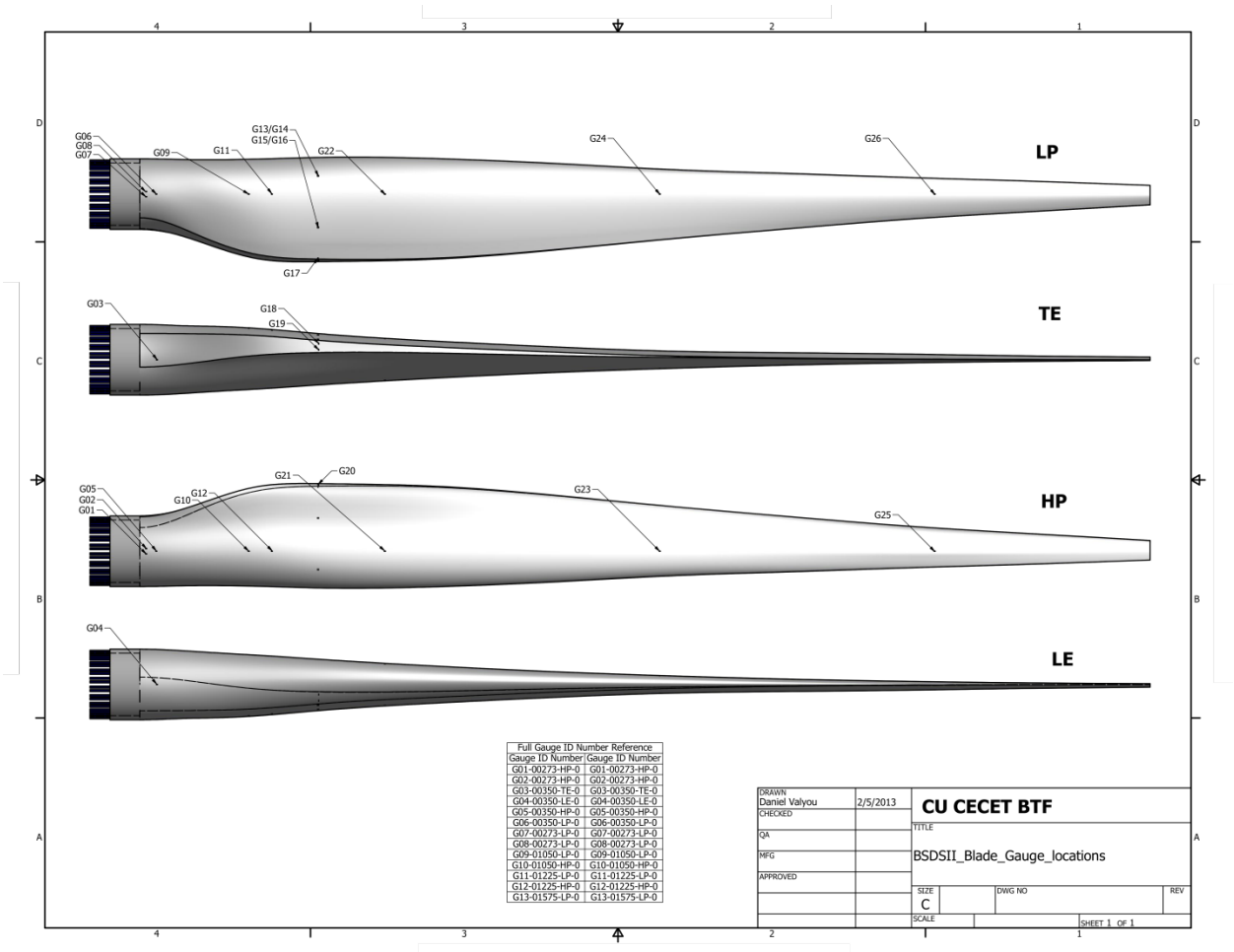

Figure 4. Blade Systems Design Studies (BSDS) blade strain gauge instrumentation

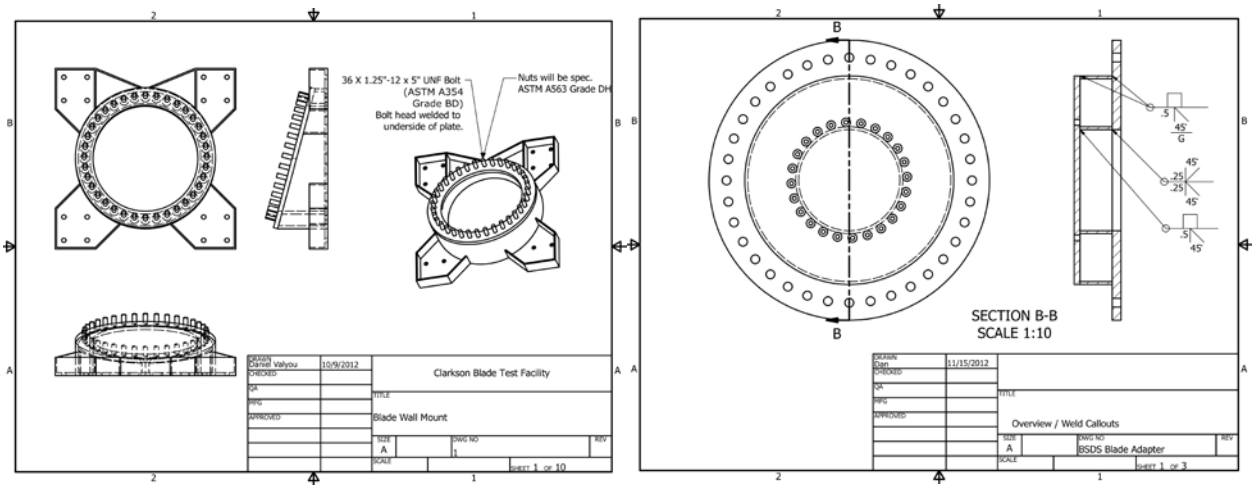

Figure 5. Blade wall mount and BSDS blade adapter

2. Saddle Design

The blade saddles (see Figure 6) are designed to be modular, with a wood insert cut to the local airfoil profile to distribute the load over the surface of the blade, which in turn is surrounded by an aluminum frame. The frame connects to the load chain through a loading arm that pivots about the blade's flapwise neutral axis, minimizing any off-axis moment introduction from the load chain. The load chain is connected to the arm through a slider that is adjusted to direct the force application through the blade's chordwise neutral axis, minimizing the introduction of a pitching moment and preventing twist caused by load introduction. Each saddle form is machined wood fitted with a 6-mm-thick soft rubber isolator between the form and the blade. Reliefs are provided at the leading and trailing edges to prevent unwanted stress concentrations.

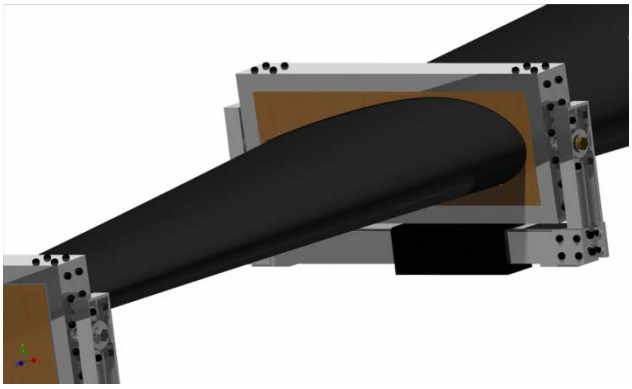

Figure 6. Blade saddle design.

3. Load Introduction Hardware

All load chains consist of 19-mm diameter, 250-kN tensile strength Dyneema synthetic wire rope. Dyneema is used because it is 8 times lighter than steel, has less recoil energy than steel, recoils in a linear fashion versus steel's snaking, and has no sharp ends when it breaks. It is also much easier to work with than steel, and can be worked with by using traditional marlinespike seamanship techniques. Connections are made with sliding eye splices and rope shackles to eyebolts attached to the load cells. The actuators are connected by means of threaded studs, eye nuts, and Supernuts that allow the connection to be torqued. The sheaves are 305-mm in diameter, include 75-mm bore bushed pulleys, and the turning block and floor plate locations are determined by test geometry.

III. BTF Coordinate System

Three coordinate systems describe the blade and blade test setup: the blade coordinate system {Xb, Yb, Zb}, the test stand coordinate system {Xt, Yt, Zt}, and the global coordinate system {Xg, Yg, Zg}. Most test information in this paper is given in global coordinates indicated by {Xg, Yg, Zg}. Specific locations on the blade including instrumentation and saddles will also make use of blade coordinates {Xb, Yb, Zb} with the blade root as the origin. Although many manufacturers refer to a rotor radius dimension measured from the center of the turbine hub, the BTF only references the blade span location measured from the root plane of the blade.

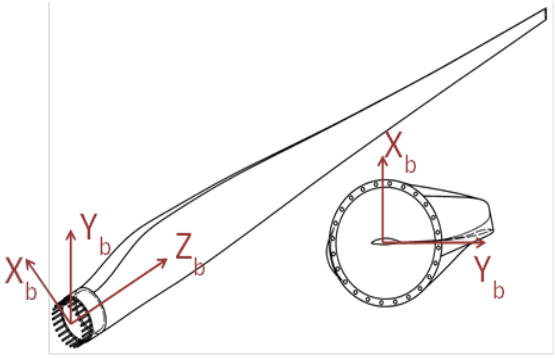

Figure 7. Blade coordinate axes.

Blade coordinate axes are defined with the origin at the center of the root as shown in Figure 7. The Xb-Yb plane is the plane of the root flange with the origin on the pitch axis. The Yb axis is in the LE – TE direction at the blade's zero angle of attack. The Zb axis is from root to tip and is also the blade's pitch axis.

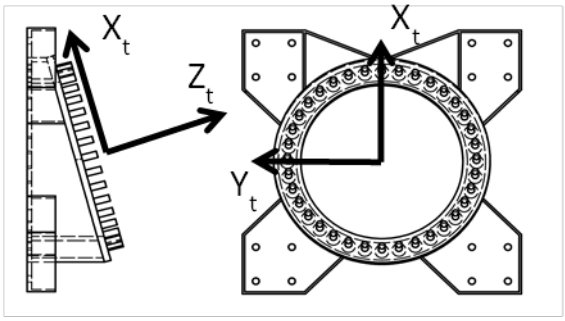

Figure 8. Test stand coordinate system.

The origin of the test stand coordinate system is at the center point of the test stand diameter, flush with the face of the test stand as shown in Figure 8. At a minimum, there is a pitch angle rotation (about Zb) and a translation because of the adapter plate and spacer thickness to convert from the blade coordinate system to the test stand coordinate system.

The global coordinate system (Figure 9) is rotated about the Yt axis and translated. The *Zg* axis is the primary axis parallel to the test laboratory blade length direction. Yg is horizontal, parallel to the laboratory floor, and Xg is vertical. The origin is located at a point level with the strong floor in the corner created by the two strong walls. The global coordinate system is rotated from the test stand coordinate system by the test stand angle about the Yt/Yg axes and translated in all three dimensions.

Blade information is typically provided in blade coordinates, which is then converted to global coordinates for calculations. The raw measurement data including deflections and force angles is measured in global coordinates. The resulting deflection is presented in global coordinates and compared to the theoretical values in that coordinate system.

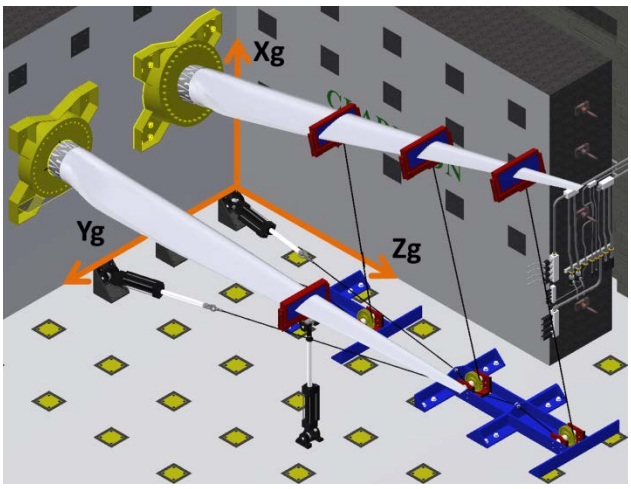

Figure 9. Global coordinate system description.

IV. The BSDS Commissioning Blade

The blade used for the commissioning of the BTF facility is the Sandia BSDS blade manufactured by TPI Composites. TPI designed and produced production molds and assembly fixtures for the BSDS prototype blades, and produced one blade in December 2012, which was shipped to Clarkson University in January 2013. The BSDS blade was designed to be a simpler-to-fabricate, less expensive, and lighter alternative to earlier 9-m blade designs. The blade is 8.325 m long from the blade root, weighs 130 kg, and has a center of gravity that is 2.83 m from the root. These specifications were given by the manufacturer upon delivery, and were verified in-house prior to instrumenting and mounting the blade. The blade was mounted in the facility for static testing, as shown in Figure 10, and for fatigue testing, as shown in Figure 11.

Figure 10. BSDS blade mounted for static testing.

Specifications for the BSDS geometry are provided in Table 3 and Table 4. The blade features a flatback airfoil for half of the blade, developing into a typical airfoil trailing edge. Flatback airfoils differ from truncated airfoils, offering the structural benefits of thicker sections without large aerodynamic losses. See Ref. 2 and Ref. 3 for information on blade design, composite specifications, and material properties. See Refs. 4–8 for information on the aerodynamics of flatback airfoils.

The blade root attachment consisted of 24 5/8-inch-18 studs extending 240 mm into the root of the blade from the root face, with the final 150 mm of the stud embedment tapered to avoid stress risers[2]. The root flange consisted of 24 13-mm-thick trapezoidal aluminum plates, which the mounting studs thread through, and are bonded to the composite blade root and each other, forming a 24-sided flange ring.

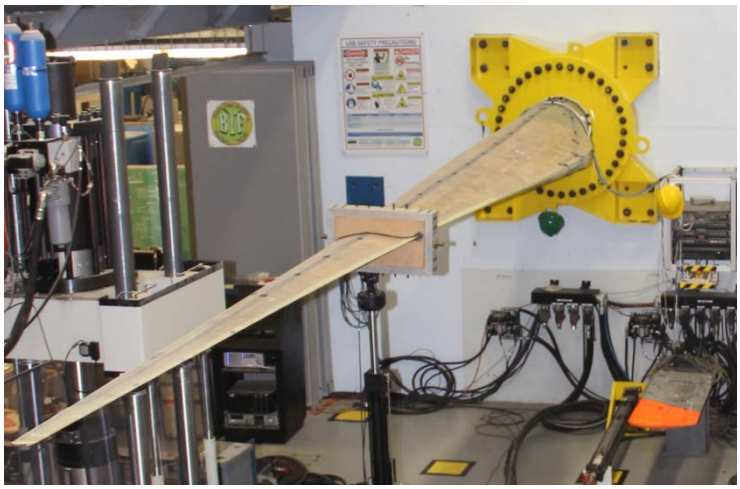

Figure 11. BSDS blade mounted for fatigue testing.

Table 3. Blade geometry details[2]

Span Length (with Hub):	9,000 mm
Blade Root Location:	7.50% span
Blade Root Location:	675 mm
Blade Length:	8,325 mm
Root Diameter (7.5% and 10% span):	20.425 inches
Root Diameter (7.5% and 10% span):	518.795 mm

Table 4. Rotor blade data[2]

FB Planform / 9.0 Meter Rotor Diameter

Blade Length (m) (ft)	8.325	27.3	Rotor Speed (rpm)	55.5
Hub Radius (m) (ft)	0.675	2.2	Wind Speed (m/s)	10.0
Rotor Radius (m) (ft)	9.000	29.5		

Station Number	Radius Ratio	Radius (mm)	Station (mm)	Chord Ratio	Twist (deg)	Chord (mm)	Thickness (mm)	Thickness Ratio	Airfoil Type	Reynolds Number
1	5%	450	449	0.0623	12.0	519	519	100.00%	Circle	3.67E+05
2	15%	1350	1349	0.0732	12.0	610	480	78.74%	FB 6300-1800	5.30E+05
3	25%	2250	2249	0.0952	11.9	792	435	54.87%	FB 5487-1216	8.93E+05
4	35%	3150	3149	0.0918	9.0	764	327	42.86%	FB 4286-0802	1.09E+06
5	45%	4050	4049	0.0788	6.4	656	225	34.23%	FB 3423-0596	1.15E+06
6	55%	4950	4949	0.0626	4.3	521	141	27.00%	FB 2700-0230	1.09E+06
7	65%	5850	5849	0.0497	2.6	414	99	24.00%	FB 2700/S830	1.00E+06
8	75%	6750	6749	0.0375	1.3	312	66	21.00%	S830	8.65E+05
9	85%	7650	7649	0.0276	0.5	230	44	19.00%	S830/31	7.18E+05
10	95%	8550	8549	0.0176	0.1	147	26	18.00%	S831	5.09E+05

V. Commissioning Test

Three commissioning tests were performed with the BSDS reference blade as part of qualifying the facility for operation. Upon receipt of the blade, a series of modal tests were performed and the blade's modal parameters were characterized. In June 2013, the commissioning static test was performed, prior to the facility's public commissioning on 8 August 2013. Finally, from mid-August to mid-September, a 30-day fatigue test was performed to complete the facility's commissioning.

A. Modal Test

As shown in Figure 12, the blade was mounted on the wall and the test conducted by exciting the structure in both the Xb and Yb directions at the intersection of the trailing edge and blade root, and the response accelerations were measured by 48 accelerometers mounted in a combination of Xb and Yb orientations.

The natural frequencies and damping ratios corresponding to this test configuration, estimated using the LMS Polymax software, are summarized in Table 5, and the corresponding mode shapes are depicted in Figure 14. Figure 13 shows a good correlation between the identified mode shapes. As Table 6 reveals, the wall-mounted blade has lower natural frequencies than published results for the free-free configuration[9]. Moreover, the free-free configuration identified additional modes.

Figure 12. Experimental setup of the wall-mounted blade.

Table 5. Modal Data for the Mounted Blade

Mode #	f_n [Hz]	ζ_n [%]	Mode type
1	3.80	0.18	IF
2	8.48	0.65	$IL + IIF$
3	9.22	0.37	IIF
4	17.9	0.51	$IIIF$
5	21.67	0.55	IIL
6	31.41	0.42	IVF
7	46.06	0.42	$VF + IIIL$
8	47.57	0.48	$IIIL + VF + IT$
9	60.04	0.5	IT
10	63.44	0.50	$VIF + IT$
11	73.12	0.53	$IIT + IVL + VIIF$
12	83.22	0.81	IVL
13	92.96	0.60	$VIIF + IIIT$
14	97.15	0.54	$IIIT$
15	110.55	0.59	$VIIIF$

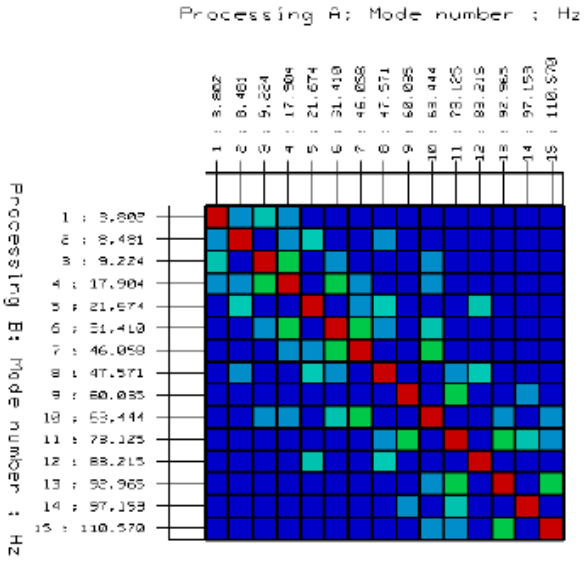

Figure 13. Auto-Modal Assurance Criterion for the mounted blade.

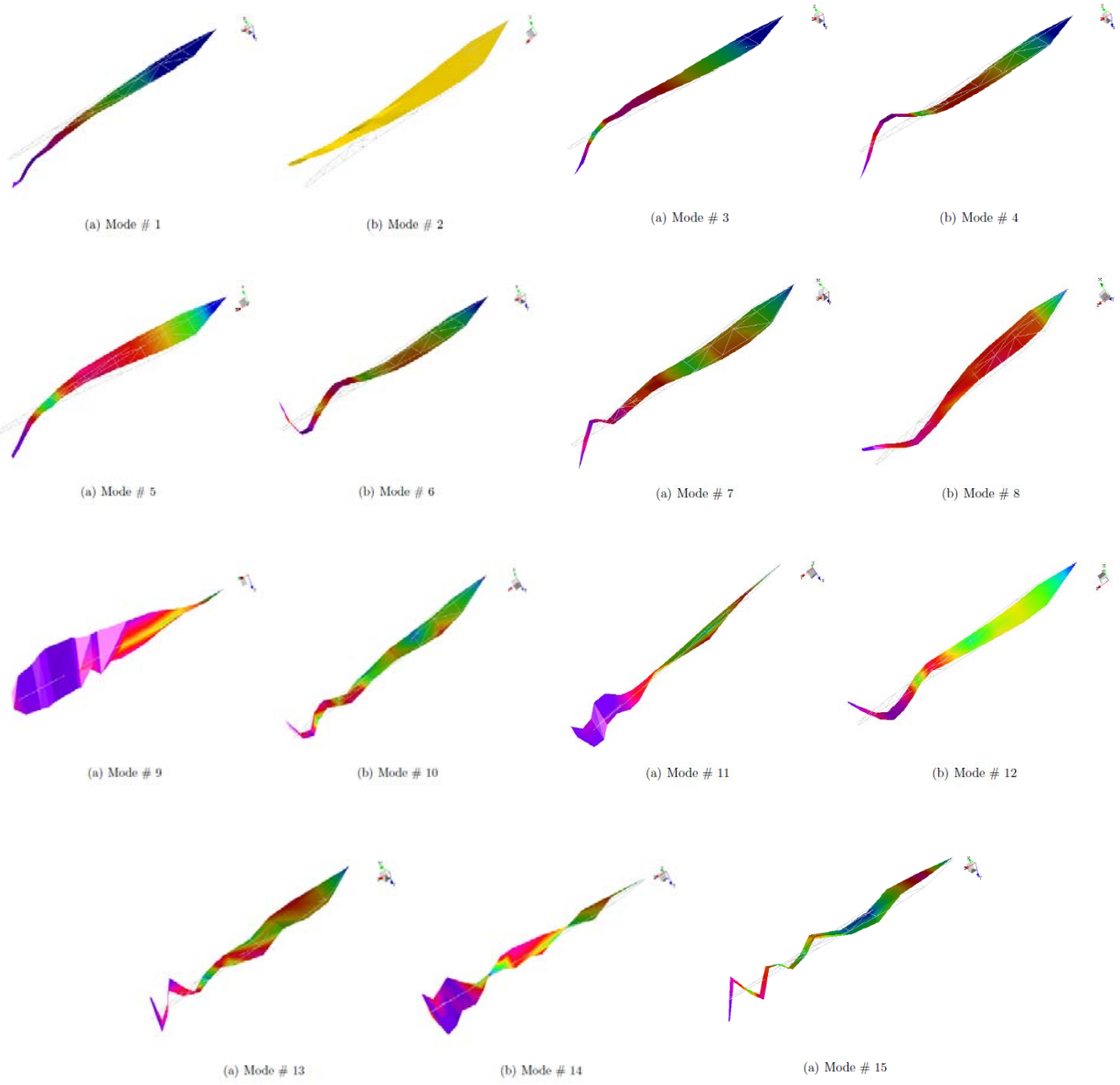

Figure 14. Normal modes estimated from the impact test for the wall-mounted blade.

Table 6. Modal data estimated in previous analyses, free-free blade[9]

Mode #	f_n [Hz]	ζ_n (%)	Mode Type
1	5.45	0.45	*IF*
2	13.5	0.43	*IIF*
3	16.5	0.97	*IL*
4	25.4	0.43	*IIIF*
5	38.6	0.6	*IVF*
6	40.1	0.94	*IIL*
7	52.5	1.2	*T*
8	65.1	0.82	*T*
9	72.1	0.72	*IIIL*

B. Static Test

Commissioning of the BTF static test capabilities took place on 27 June 2013. The test was performed to 75% of the BSDS blade design loads in the positive flapwise direction, with three load introduction points. The design load, test load approximation, and load introduction geometry are similar to those given in Ref. 10. The BTF laboratory design enables testing to be conducted in the vertical downward direction with independent actuators for each saddle. This is the typical approach used by many laboratories for full-scale testing of larger multi-megawatt-scale wind turbine blades today. By comparison, the NREL test in 2007 used a whiffletree to distribute the load from a single overhead crane to the three saddles and the load was applied against gravity in the upwards direction[10]. The whiffletree approach was more common historically and is often used for static tests on smaller blades that exhibit limited deflection. Test loading for the commissioning test of the BTF is shown in Table 7.

Table 7. Commissioning test loading data

Saddle Number (Control Channel Number)	Saddle Span Location (m)	Saddle Target Compression (kN)	Predicted Saddle Mass (kg)	Predicted Load Chain Mass (kg)	Live Force (kN)
1	3	10	50	15	9.79
2	4.8	4	40	5	3.96
3	6.6	3.75	30	5	3.65

1. Test Simulation Results

The design loading, mass matrix, and stiffness matrix for the BSDS blade were interpolated to 1001 points and analyzed using a finite-beam-element model in Microsoft Excel. This model is used to estimate the actual load applied at each point, the fraction to target loading, and the deflection of the blade under 100% load. The results are used to ensure the fraction to target load is maintained as close as possible to one over the largest possible blade span, and to predict the optimal turning block locations to obtain perpendicular load introduction at 100% load. The results of the loading simulation are shown in Figure 15, and the blade's predicted deflection under load is shown in Figure 16.

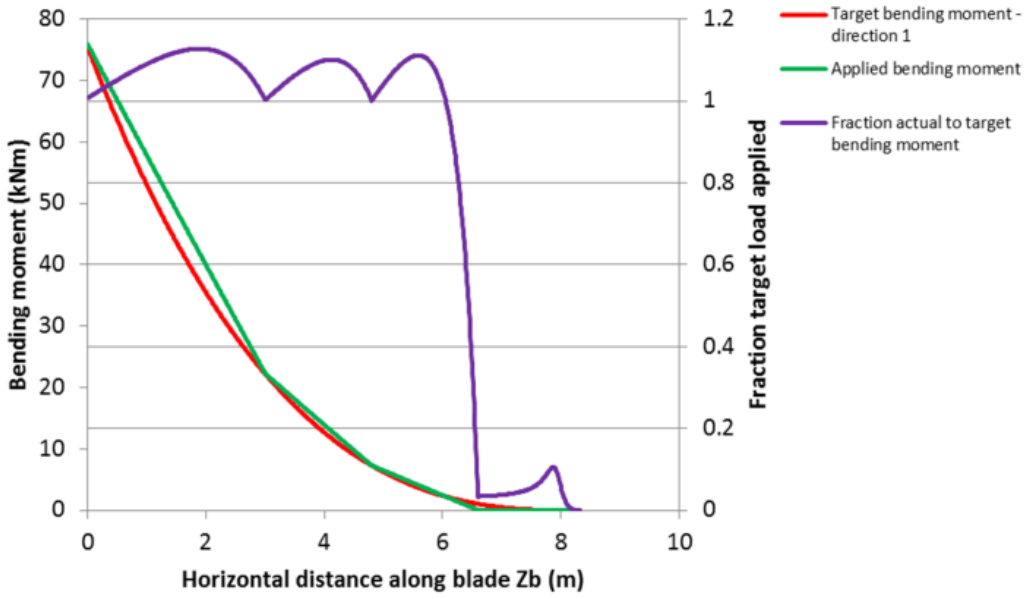

Figure 15. Blade loading simulation results.

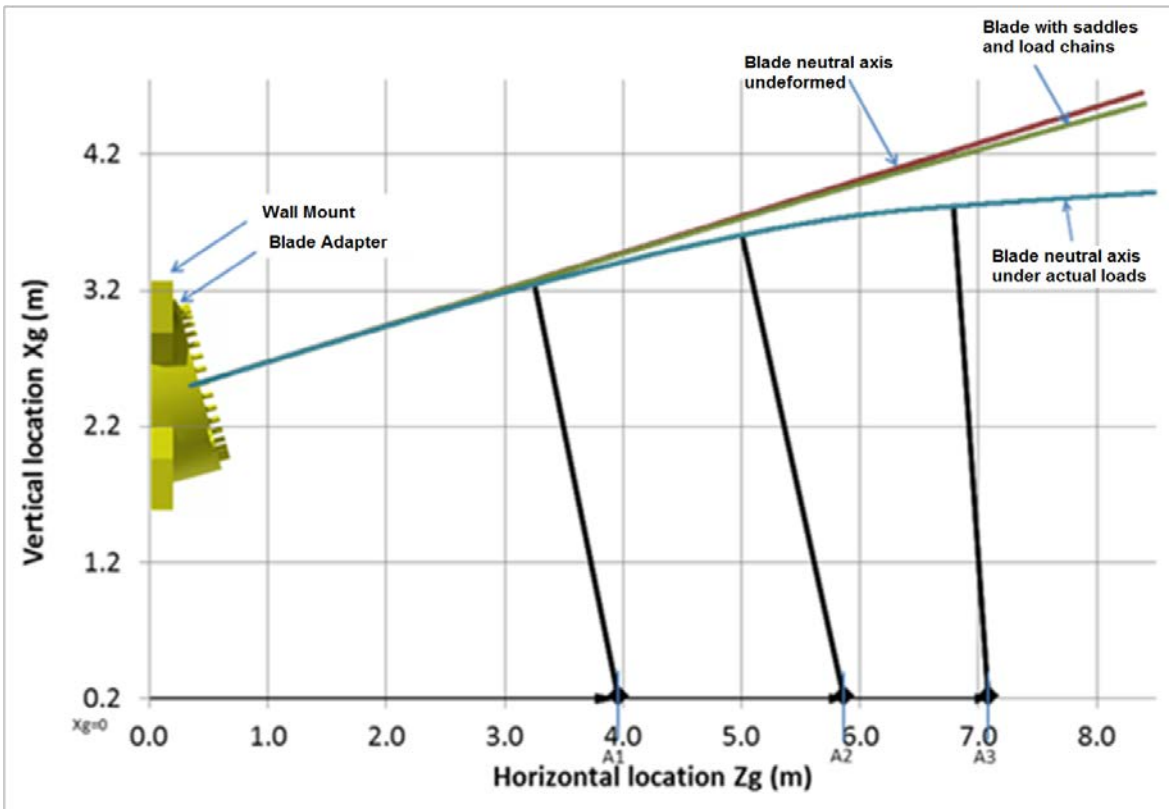

Figure 16. Blade deformation simulation results.

The test results match closely to published data. The spar cap strains at 100% load were compared with those for the test described in Ref. 10 (Figure 17).

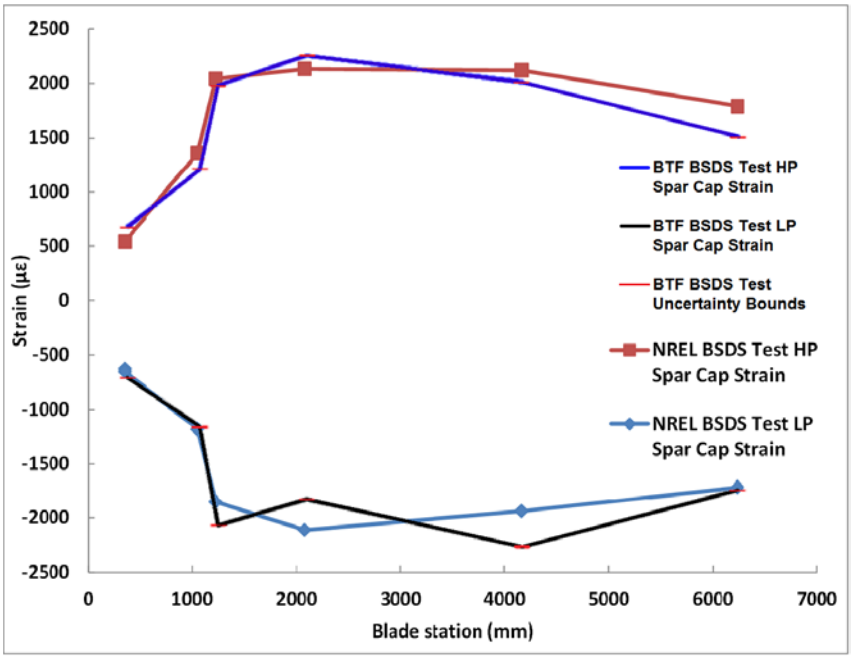

Figure 17. Blade spar cap strains at 100%load (54.36 kN-m) compared to past test of BSDS blade at NREL at a similar load level.

Both blades showed similar strain distributions at a similar load level. Because the BTF commission test was conducted in the direction of gravity and the cables were setup to pull perpendicular to the saddles in the deformed position while the NREL test was configured to load against gravity and loaded the saddles approximately perpendicular to the unreformed blade, the load states in the two tests are not identical[10]. However, the final bending moment distribution is similar enough between the two tests that comparing the strain distribution along the blade is reasonable. Each BTF data point in Figure 17 represents the mean of 30 seconds of data at the specified load level, sampled at 64 hertz (Hz). The error bars represent one standard deviation from the mean. NREL data points represent the values recorded at a single point in time without any averaging. Throughout the test at the BTF, the blade displacement remained linear and showed low hysteresis (Figure 18). Spar cap strains (Figure 19) were also linear. Three replicates were performed for the static test, and the results demonstrated tight uncertainty bounds for the 95% confidence interval of the mean, as a result of the low noise and excellent signal conditioning of the DAQ system.

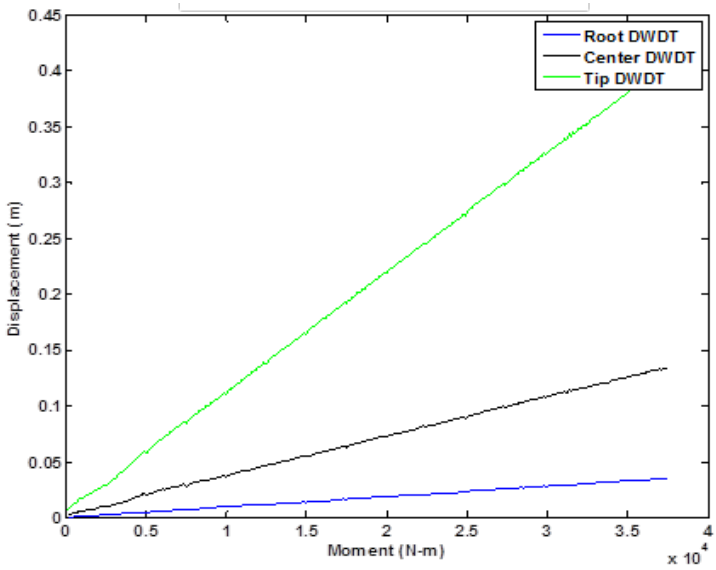

Figure 18. Blade displacement versus moment.

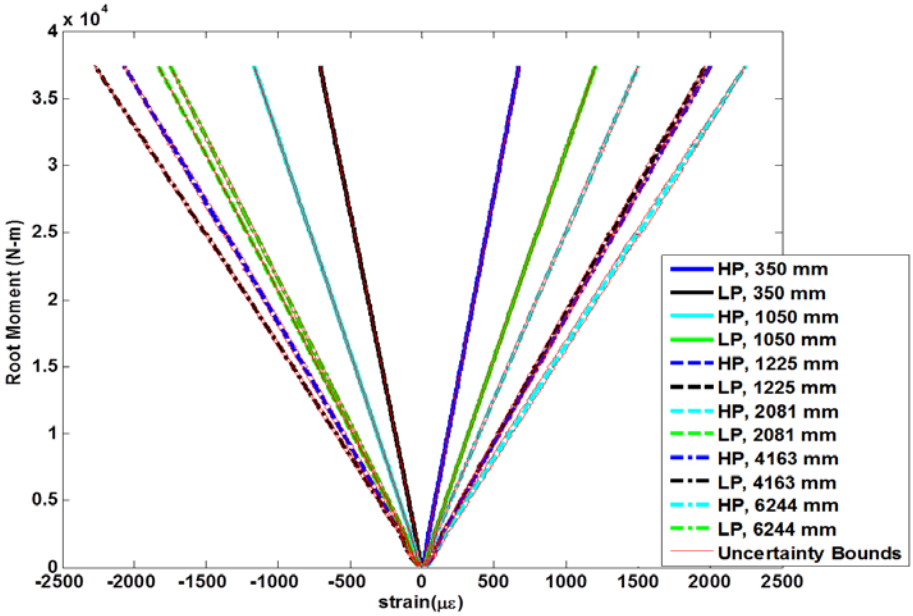

Figure 19. Spar cap strain versus moment.

C. Fatigue Test

The fatigue commissioning test was conducted between 13 August 2013 and 14 September 2013. The experiments performed included a flapwise fatigue blade test to 8.85×10^5 cycles and a post-fatigue, strain-to-moment calibration test. The test was a force-displacement, single actuator test with load introduction at the 4.8-m blade station. The dynamic actuator was bolted directly to the blade saddle frame through a monoball joint. The fatigue maximum live loading applied to the blade was 6000 N, with r=0.1, dictating a minimum live load of 600 N. The target test loading was selected through consultation with NREL to correspond to test loads performed by the lab in the past. Periodically during the fatigue test, and after completion, a static test load was applied with the fatigue actuator to calibrate the response of the strain gauges and determine a strain-to-local-moment relationship. This calibration was used as a second metric for observing changes in local stiffness over time, and enabled the use of the strain gauges as moment gauges.

A similar 1 million-cycle force-displacement flap fatigue test was conducted on a Sandia BSDS blade at NREL in 2008. The actuator saddle location was at the 4.8-m blade station and a load reversal ratio of R=0.1 was used with a maximum target load of 6300 N. The NREL test was performed in displacement control with the displacement amplitude and mean adjusted every few days throughout the test to maintain the target loads.

Overall, the BTF fatigue test displayed a barely detectable 0.35% reduction in stiffness over the course of the test, as shown in Figure 20. The dynamic stiffness is defined as the ratio of the load range to the displacement range for a given cycle. Each data point in the BTF data represents the average normalized stiffness over 10,000 cycles and the error bars are 1 standard deviation for those cycles. Figure 20 also shows historical comparison data to a flap fatigue test performed at NREL in2008. The NREL data was down-sampled for plotting without any averaging. The down-sampled normalized data from the 2008 BSDS test at NREL nearly all lies within one standard deviation of the mean of the data collected at Clarkson, as shown in Figure 20.

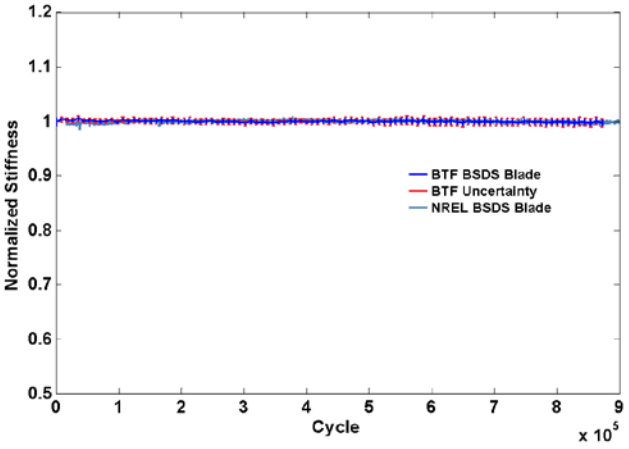

Figure 20. Comparison of the dynamic stiffness during fatigue testing of BSDS blades at the BTF and NREL.

Figure 21 shows the normalized "strain stiffness" measured at each gauge during the BTF fatigue test, defined as the change in blade strain with change in fatigue load for each cycle. To calculate the error bars, a histogram was taken of the data. Sampled at 64 Hz, each bin represents 5.6×10^5 samples. The error bars represent one standard deviation from the mean for each bin. The location of each gauge can be determined by cross-referencing the legend entries with the key in Section II.B.1. The one notable gauge was gauge G25, at a 6.244-m span on the HP side, whose stiffness deviated wildly from the other gauges. It was the only functioning gauge outboard of the load introduction point at 4.8 m. The corresponding LP gauge failed, but was not repaired because the blade outboard of 4.8 m was not tested. The loading of G25 was purely inertial, and increased with time as blade stiffness decreased. All other gauges accurately reflected the global stiffness of the blade.

At the conclusion of testing, a post-test static load was applied to the blade with the fatigue actuator. The relation between strain and the local bending moment is shown in Figure 22. This figure shows the raw data, curve fit of the data (solid line), and the 95% confidence interval of the curve fit (dashed lines). As can be seen by the wider spread of the 95% confidence interval compared to Figure 19, this test gives a less precise measure of the blade's strain-to-moment relation than the full static test. This reduction in precision is because the moment distribution was lower, the blade was only loaded at a single point, and it was loaded more rapidly in a linear rather than a null-paced stepped fashion; however, the results correspond to the strain measurements taken in the static test prior to fatigue loading, indicating no significant loss in stiffness. All the strain-to-local-moment relations are linear, which also corresponds to the results of the static testing.

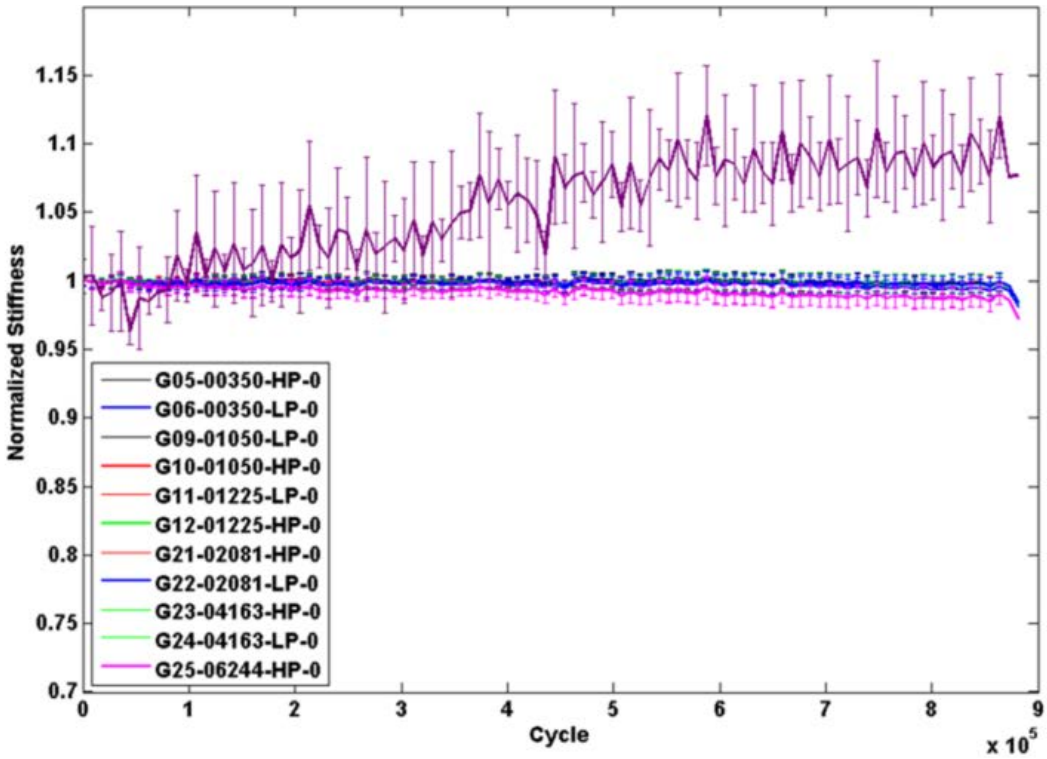

Figure 21. BTF BSDS spar cap stiffness.

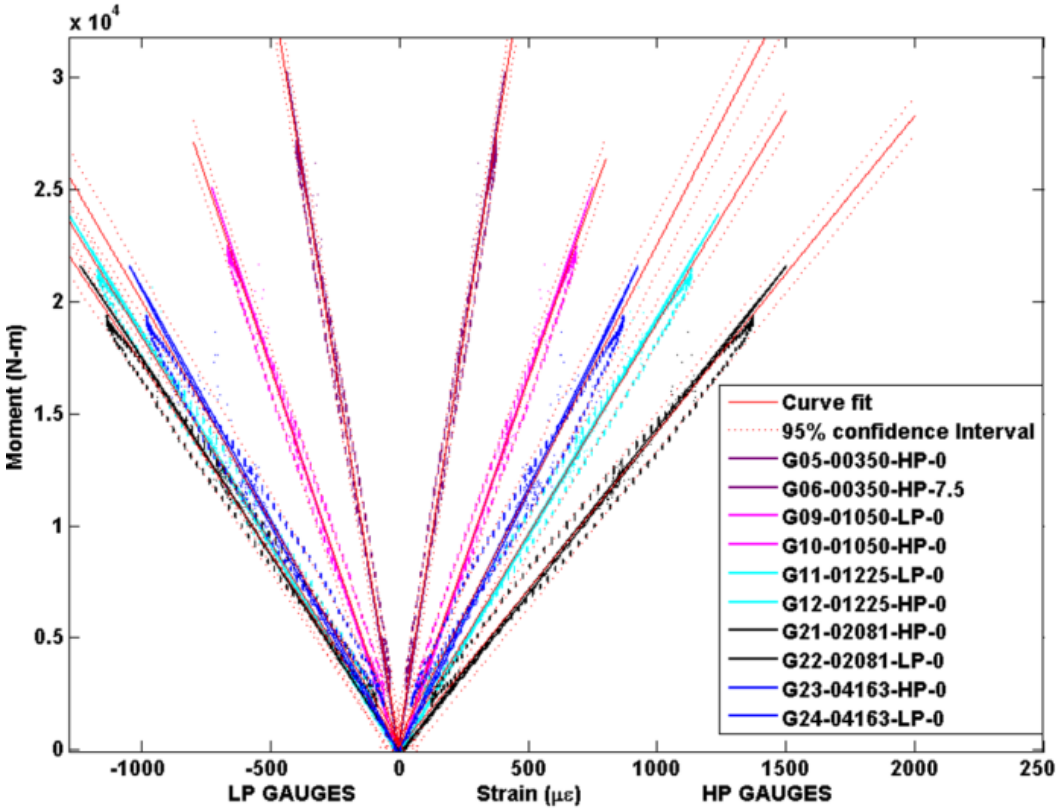

Figure 22. BTF BSDS spar cap strain versus moment following the fatigue test.

VI. Conclusion and Continuing Work

This work discussed the Clarkson University/CECET Blade Test Facility, including its design, control, and instrumentation systems. The results of the facility's commissioning blade test utilizing a Sandia BSDS reference blade were presented. Commissioning test data were compared to data for structural testing experiments on BSDS blades conducted at NREL in 2007 and 2008. What follows are the lessons learned from this work. The modal, static, and fatigue test results of the BSDS blade agreed well with historical test data. The modal analysis showed that the mounted blade has lower natural frequencies than the free boundary condition tested in previous analyses. This suggests that matching the mounted blade configuration in modal testing is essential to predicting the first natural frequency, which is critical for planning the fatigue test driving frequency. The static blade testing results closely matched historical data, and the fatigue test trends agreed with historical data. The results of individual measurements indicated low signal-to-noise ratio and tight error bounds/confidence intervals for the data collected during these tests.

Following the commissioning testing, the CECET BTF is now operational and several blade test projects are in progress and preparation. Development of the BTF's bi-axial fatigue test system is underway and expected to be complete by the end of spring 2015. Plans are currently in progress to expand the BTF's scope as well as conduct the first structural test of an aircraft structure (fully composite monocoque unmanned aerial vehicle wing). In addition, research is currently underway to develop new test instrumentation that will greatly increase strain data acquisition density, enabling a more comprehensive strain characterization of structures such as wind turbine blades and aircraft wings.

Acknowledgments

The authors would like to thank the generous financial support of the New York State Energy Research and Development Authority (NYSERDA) under grant agreement # 18460, and the commitment made by the Center for Evaluation of Clean Energy Technologies and Intertek, along with the support and fruitful discussions with Stephen Nolet at TPI Composites, Inc. We would also like to acknowledge MTS, LMS, and PCB for training, technical consultancy, and support.

The work performed in 2007 and 2008 generating the Sandia BSDS blade test data used for comparison purposes in this paper was supported by the U.S. Department of Energy under Contract No. DE-AC36-99GO10337 with the National Renewable Energy Laboratory. Funding for this work was provided by the DOE Office of Energy Efficiency.

References

[1]Hahn, B., Durstewitz, M., Rohrig K., "Reliability of Wind Turbines," *Wind Energy*, Springer Berlin Heidelberg: New York, 2007; pp. 329–332, http://renknownet2.iwes.fraunhofer.de/pages/wind_energy/data/2006-02-09Reliability.pdf.

[2]Berry, D. S., Berg, D. E., "Blade System Design Studies Phase II: Final Project Report," SAND08-4648, Printed July 2008, http://windpower.sandia.gov/other/084648.pdf.

[3]Griffin, D., Ashwill, T. D., "Blade System Design Studies Part II: Final Project Report (GEC)," SAND09-0686, Printed May 2009, http://windpower.sandia.gov/other/090686.pdf.

[4]van Dam, C. P., Kahn, D. L., Berg, D. E., "Trailing Edge Modifications for Flatback Airfoils," SAND08-1781, http://prod.sandia.gov/techlib/access-control.cgi/2008/081781.pdf .

[5]van Dam, C. P., Mayda, E. A., Chao, D. D., Berg, D. E., "Computational Design and Analysis of Flatback Airfoil Wind Tunnel Experiment,"SAND08-1782, http://prod.sandia.gov/techlib/access-control.cgi/2008/081782.pdf.

[6]Baker, J. P., van Dam, C. P., Gilbert, B. L., and Berg, D. E., "Flatback Airfoil Wind Tunnel Experiment," SAND08-2008, http://prod.sandia.gov/techlib/access-control.cgi/2008/082008.pdf.

[7]Berg, D. E., Barone, M. "Aerodynamic and Aeroacoustic Properties of a Flatback Airfoil (Will it Rumble or Whisper?)" Windpower 2008, Houston, Texas, June 2008, http://windpower.sandia.gov/other/AWEA-06-08-Berg.pdf.

[8]Berg, D. E., and Zayas, J. R., "Aerodynamic and Aeroacoustic Properties of Flatback Airfoils," 46th AIAA Aerospace Sciences Meeting and Exhibit (27th ASME Wind Energy Symposium), Reno, Nevada, January 2008, http://windpower.sandia.gov/asme/AIAA-2008-1455.pdf.

[9]Griffith, D. T., andCarne, T. G., "Experimental Uncertainty Quantification of Modal Test Data," XXV IMAC, Orlando, Florida, USA, February 19–22 2007, http://sem-proceedings.com/25i/sem.org-IMAC-XXV-s02p02-Experimental-Uncertainty-Quantification-Modal-Test-Data.pdf.

[10]Paquette, J., van Dam, J., and Hughes, S., "Structural Testing of 9 m Carbon Fiber Wind Turbine Research Blades," 45th AIAA Aerospace Sciences Meeting and Exhibit, Reno, Nevada, USA, January 2007, http://windpower.sandia.gov/asme/AIAA-2007-Testing9m.pdf.